Research Article | Vol. 28, No. 12 / 8 June 2020 / Optics Express 18172
Optics EXPRESS

1.55 μm electrically pumped continuous wave lasing of quantum dash lasers grown on silicon

YING XUE,[1,2] WEI LUO,[1,2] SI ZHU,[1] LIYING LIN,[1] BEI SHI,[1] AND KEI MAY LAU[1,*]

[1] *Department of Electronic and Computer Engineering, Hong Kong University of Science and Technology, Clear Water Bay, Kowloon, Hong Kong, China*
[2] *Y. Xue and W. Luo contributed equally to this work*
[*] *eekmlau@ust.hk*

Abstract: Realization of fully integrated silicon photonics has been handicapped by the lack of a reliable and efficient III-V light source on Si. Specifically, electrically pumped continuous wave (CW) lasing and operation sustainable at high temperatures are critical for practical applications. Here, we present the first electrically pumped room temperature (RT) CW lasing results of 1.55 μm quantum dash (QDash) lasers directly grown on patterned on-axis (001) Si using metal organic chemical vapor deposition (MOCVD). Adopting a dash-in-well structure as the active medium, the growth of QDash was optimized on an InP on Si template. Incorporating the advantages of the optimized material growth and device fabrication, good laser performance including a low threshold current of 50 mA, a threshold current density of 1.3 kA/cm^2 and operation at elevated temperature up to 59 °C in CW mode was achieved. Comparison of lasers grown on Si and native InP substrates in the same growth run was made. Based on the laser characteristics measured at room temperature and elevated temperatures, the QDash quality on the two substrates is comparable. These results suggest that MOCVD is a viable technique for lasers on Si growth and represent an advance towards silicon-based photonic-electronic integration and manufacturing.

1. Introduction

The exponential growth of data communication traffic has triggered rapid development of silicon photonics in the past two decades. Si photonics promotes the integration of optical components and electronic building blocks on the same chip with mature and cost-effective complementary metal-oxide-semiconductor (CMOS) technologies [1–3]. Intensive research and improvement have been demonstrated on Si-based photonic devices [4–6]. After successful incorporation of passive devices, an efficient laser source on Si is the nub for fully integrated Si photonics. III-V lasers with excellent optical characteristics that have been used for decades in telecommunication were deemed to be the feasible solution for on-chip lasers. Bonding technique has been successfully used to address the issue of integrating III-V lasers on Si. Remarkable laser performance has been demonstrated using bonding-based techniques in recent years [7]. For the long term perspective, however, direct epitaxy growth for integration is expected to offer larger scalability, lower cost and better fabrication compatibility [8,9]. It is challenging to directly grow these high gain III-V alloys on Si due to the large lattice mismatch that will introduce defects and degrade the device performance severely [10,11]. To help mitigate the issue, the conventional quantum well (QW) gain medium can be replaced with one-dimensional atom-like quantum structures such as quantum dot (QD) and quantum dash (QDash) for confinement of carriers [12,13]. Their merits include lower sensitivity to crystalline defects, less power consumption, and higher temperature stability [14]. To date, III-V QD lasers on Si grown by molecular-beam epitaxy (MBE) emitting in 1.3 μm band have been well established, with low threshold, high operation temperature, and excellent lifetime [2,15–17]. However, it is challenging to extend the emission wavelength of these GaAs-based lasers to 1.55 μm [18]. Alternatively, MOCVD

#392120 https://doi.org/10.1364/OE.392120
Journal © 2020 Received 5 Mar 2020; revised 19 Apr 2020; accepted 25 May 2020; published 3 Jun 2020

Optics EXPRESS

grown InP-based lasers can emit light at both 1.3 μm and 1.55 μm by minor tuning of the QDash growth parameters. Meanwhile, the manufacturability value of MOCVD also makes it attractive to be the candidate for integrated laser growth. In the earlier work, our group has demonstrated room temperature (RT) optically pumped and RT electrically pumped pulsed lasing at 1.55 μm of the QD and QW lasers grown on Si [19–21]. However, for practical applications, electrically pumped CW lasing is required, and the capability of high temperature operation is essential to cope with the heat generated by the electricity on chips.

Here we report the first electrically pumped CW lasing results of InAs/InGaAs/InAlGaAs QDash lasers directly grown on silicon emitting at 1.55 μm by MOCVD. Using a modified InAs/InGaAs/InAlGaAs dash-in-well structure, light confinement was enhanced, thereby facilitating CW lasing of the on Si lasers. Furthermore, the fabricated narrow-ridge waveguide lasers were deeply etched through the active region to maximize optical confinement and minimize current spreading. Incorporating these optimizations, the QDash lasers on Si demonstrate much improved performance with the lowest threshold of 50 mA measured on devices with 0.5 mm length and lowest threshold current density of 1.3 kA/cm^2 on devices 1.5 mm long under CW current injection. High temperature CW lasing up to 59 °C with steady quantum efficiency was presented. Our lasers on Si show comparable performance to those on InP in terms of static characteristics which is shown by the parametric study. These advances make a major step towards offering full photonic functionality on Si.

2. Material growth and laser fabrication

In this work, V-groove patterned on-axis (001) Si substrates were used for growth [22]. The entire laser structure and buffer layers were grown by MOCVD in an Aixtron AIX-200/4 system. 1.1 μm GaAs was grown on the V-groove patterned Si substrate as intermediate buffer [23]. After the GaAs growth, root-mean square (RMS) roughness of surface atomic force microscope (AFM) image is around 1.1 nm. Then a 3.1-μm InP buffer layer with 3 sets of 10-period $In_{0.63}Ga_{0.37}As$ (12 nm)/InP (34 nm) strained-layer superlattices (SLSs) inserted were grown subsequently. AFM root-mean square roughness around 2 nm was achieved after the growth of the InP buffer, which provides a smooth growth front for the following laser structure. The threading dislocation density after the growth of InP buffer is 3.6×10^8/cm^2, determined by plan-view transmission electron microscopy (TEM). The complete laser structure is schematically delineated in Fig. 1(a), 600 nm InP n-contact layer and 630 nm InP n-cladding layer were grown with doping parameter detailed in Ref. [23]. A three-layer InAs/InGaAs dash-in-a-well structure embedded in InAlGaAs separated confinement heterostructure was utilized for the active region. A 1500 nm Zinc-doped InP p-cladding layer and a 140 nm $In_{0.515}Ga_{0.485}As$ p-contact layer were finally deposited. Figure 1(b) shows the TEM image of the three layers of QDashes. Growth of the active region was optimized based on the photoluminescence (PL) and AFM characterization. The Al composition of the InAlGaAs is 0.24 and low temperature InGaAs is used as the cap layer. Compared with previously reported growth, an increase of the PL intensity and reduction of the full width at half maximum (FWHM) of the spectrum were obtained. The RT PL of the optimized QDashes on V-groove Si and native InP without cladding and contact layers are presented in Fig. 1(c). FWHM of around 80 meV was estimated for both samples. QDash observed by AFM is shown in the inset of Fig. 1(c) with an estimated density of 3.2×10^{10} cm^{-2}. Identical laser structure was also grown on InP native substrate in the same growth run and fabricated along the same direction for comparison [24].

Deep etched narrow ridge-waveguide lasers were fabricated on the as-grown samples with cavity widths of 2, 4, 6, 8 μm. Ridge waveguides were defined using conventional photolithography and subsequent one-step inductively coupled plasma (ICP) etching with a total etching depth of around 3.1 μm. Ti/Pt/Au and Ge/Au/Ni/Au were deposited as p and n-contacts followed by 550 nm SiO_2 passivation. Finally, after the metal pads formation, laser bars were cleaved and tested

Optics EXPRESS

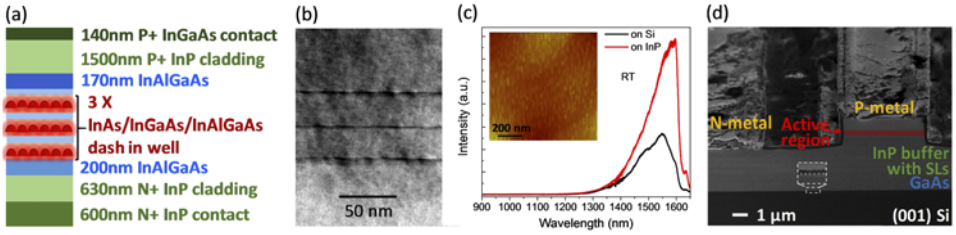

Fig. 1. (a) Complete laser structure schematic consist of 140 nm p-doped InGaAs contact, 1.5 µm p-doped InP cladding, three layers of InAs/InGaAs/InAlGaAs dash-in-well sandwiched by upper and lower InAlGaAs, 630 nm n-doped InP cladding and 600 nm n-doped InP contact; (b) TEM image of three layers of QDashes; (c) Room temperature PL of three-layer QDashes grown on Si and InP, inset: QDashes observed by AFM; (d) Tilted-view SEM of the fabricated device of 6 µm width with zoomed-in patterned V-groove Si.

with the facets uncoated. The as-cleaved lasers with various cavity lengths from 0.5 mm to 2 mm were characterized. The scanning electron microscope (SEM) image in Fig. 1(d) presents the cross-sectional view of a finished device with a 6-µm wide ridge. Multilayer stacking growth structure with zoomed-in tooth-like V-groove Si can be clearly observed. The vertical and smooth sidewall enables a low optical scattering loss.

3. Results and discussion

The as cleaved laser bars were positioned on a heatsink with a temperature controller and electrically driven by a current source in CW mode. Figure 2(a) plots a representative room temperature light-current-voltage (L-I-V) characteristic of a laser on Si with 6 µm cavity width and 1.5 mm cavity length. A threshold current density of 1.3 kA/cm^2 and a total output power in excess of 44 mW were demonstrated. And a low threshold current of 50 mA was achieved on a smaller device (2 µm width, 0.5 mm length). In the inset of Fig. 2(a), the p-i-n laser diode shows I-V characteristic with 0.7 V turn-on voltage and ~5 Ω series resistance. The room temperature emission spectra from a 2 µm × 2mm device, measured by coupling output light into a lensed fiber connected to an optical spectrum analyzer is presented in Fig. 2(b). The peak of the envelope first blue shifts with carrier injection below the threshold. Then one peak dominants at higher current injection level and finally lase at 1580 nm. The red shift of the lasing wavelength from the original PL peak is due to the thermal induced index change. Single mode lasing with extinction ratio over 21 dB within a certain current injection range was observed on the devices with narrow ridges (2 µm, 4 µm).

In the early work, we used the shallow etched structure with two mesas typically used for QW lasers to reduce the optical losses caused by sidewalls [25]. In this wok, deep etched structure was preferred for a superior optical mode confinement as the losses caused by sidewalls can be suppressed by the reduced carrier diffusion length of QDash. To confirm, devices of both structures with various cavity widths and lengths were fabricated in the same QDash direction on the samples in the same growth run for comparison of laser performance. With the same device dimensions, the deep etched QDash lasers on Si manifest lower threshold currents under CW current injection, which is consistent with the better optical confinement and reduced current spreading effect. Figure 3(a) depicts the architecture of these two structures in cross-sectional view. Figure 3(b) gives the comparison of the deep etched and shallow etched lasers with 2 mm cavity length and different cavity widths.

To benchmark the lasers on Si, more parametric investigation on the QDash lasers on Si and native InP substrates were performed. Figure 4(a) illustrates a series of L-I curves measured from the lasers grown on Si and InP. The threshold current densities of our QDash lasers on InP

Optics EXPRESS

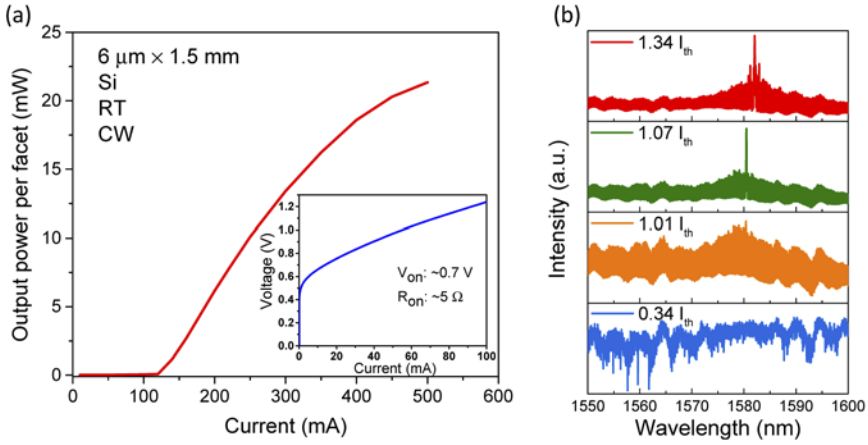

Fig. 2. (a) L-I curve of QDash laser on Si with device dimension of 6 µm width and 1.5 mm length, inset: I-V characteristic of the laser diode; (b)Room temperature electroluminescence spectrum in log scale showing ground state lasing at 1580 nm from a device of 2 µm width and 2 mm length.

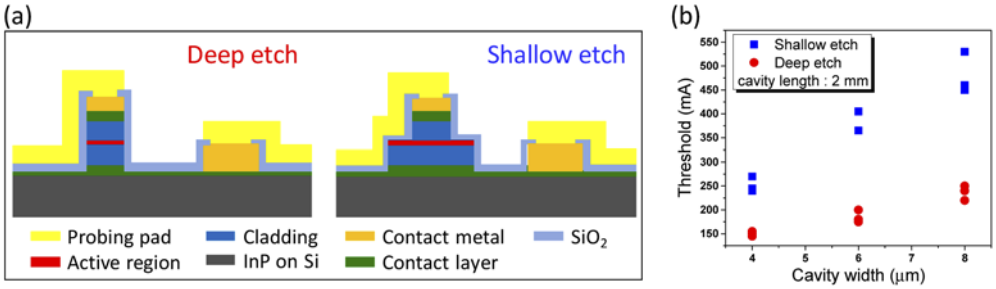

Fig. 3. (a) Schematic of finalized devices with deep etched structure and shallow etched structure in cross-sectional view; (b) Threshold currents plotted as function of various cavity widths with 2 mm cavity length for the two different structures.

are somewhat lower than the reported 1.55 µm QD lasers on InP with similar device dimensions [26,27]. Figure 4(b) reveals the clear trend of threshold drop with cavity size shrinkage for all the lasers. Statistically, similar thresholds of our lasers on both substrates were obtained. We attribute the comparable thresholds to sufficient gain of the laser active layers and good crystalline quality of the InP/Si buffer. For practical applications, on-chip lasers must be able to function at elevated temperatures in CW mode with minimal cooling. Our fabricated lasers on Si and InP can lase up to 59 °C and 65 °C under CW operation, respectively. Measured L-I curves of lasers on Si and InP at progressively increasing heatsink temperatures were plotted in Fig. 5(a) and Fig. 5(b), respectively. By fitting the increase in threshold using the exponential formula of $I_{th}(T_1)/I_{th}(T_2) = \exp(\Delta T/T_0)$, characteristic temperature T_0 was extracted to be ~44.8 K from 25 °C to 50 °C and 27.11 K from 50 °C to 59 °C for QDash laser on Si (inset of Fig. 5(a)). And the T_0 for QDash laser on InP was found to be ~41 K from 25 °C to 60 °C as exhibited in the inset of Fig. 5(b). No significant slope efficiency drop was observed with the temperature increase. For pulsed measurements, a duty cycle of 0.5% and pulse width of 400 ns were used. Output power in excess of 360 mW and threshold current density of 555 A/cm^2 were obtained in pulsed mode for lasers on Si. Pulsed lasing sustained for the lasers on both Si and native InP up to 100 °C, the upper limit of the temperature controller. Characteristic temperatures measured

Optics EXPRESS

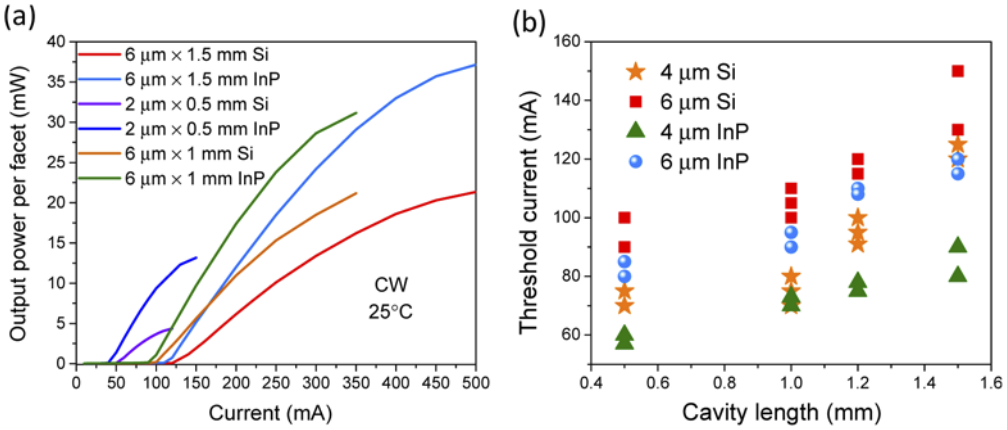

Fig. 4. (a) L-I curves of lasers on Si and native InP substrate; (b) Threshold current distribution of QDash lasers on Si compared with lasers on InP at various cavity lengths and widths.

under pulsed current injection are 60.6 K and 61.1 K for lasers on Si and InP, respectively. For a detailed statistical analysis of the high temperature performance, temperature-dependent internal parameters including internal quantum efficiency (IQE) and internal loss were investigated. Sufficient length-dependent L-I measurements at various temperatures were conducted first for a reliable calculation and fair comparison. Then the inverse of differential quantum efficiency was derived from the slope of the L-I curves and plotted versus cavity length. By fitting these experimental data following the equation of

$$\frac{1}{\eta_d} = \frac{\alpha_i L}{\eta_i ln(1/R)} + \frac{1}{\eta_i},$$

where R represents the mean mirror reflectivity which is 0.32 for our InP-based cleaved facets, η_d stands for the differential quantum efficiency, and L is the cavity length, IQE η_i and internal loss α_i were extracted (see Fig. 6(a) inset and Fig. 6(b) inset). IQE and internal loss as function of CW operation temperature were plotted in Fig. 6(a) and Fig. 6(b) for lasers on Si and InP, respectively. The slight change of IQE and internal loss with the increase of temperature indicate a high temperature stability. And only limited disparity on internal loss can be noticed when comparing these parameters of the lasers on the two different substrates. Meanwhile, these parameters are roughly in line with the values of the reported 1.55 μm QD lasers on InP [26,28]. These results further corroborate a low defect density in the active region of QDash lasers on Si by dint of a high buffer quality and well optimized growth condition. Figure 6(c) shows the temperature dependence of the primary lasing mode at a fixed injection current. The lasing peak red shifts by 0.13 nm/°C (on Si lasers) and 0.14 nm/°C (on InP lasers) with the increasing temperature as the refractive index depends on the temperature. These excellent values are less than those reported in [26,27,29], which can be attributed to the high temperature stability of QDashes and small number of QDashes layers. And the linear shift implies a stable emission of ground state. Due to self-heating, slightly red shift was also observed with the increase of injection current with a factor of 0.03 nm/mA and 0.015 nm/mA for on Si and on InP ones, respectively. The thermal impedance $(d\lambda/dP)/(d\lambda/dT)$ of the device was calculated by dividing $d\lambda/dP$ measured under CW condition by $d\lambda/dT$ measured under pulsed condition [30]. Values of 35 °C/W and 33 °C/W were obtained for lasers on Si and InP, respectively. These values are somewhat higher than the reported 26.76 °C/W for InAs/InP QD Fabry-Perot lasers on InP [31]. Compared with the well-developed 1.3 μm lasers on Si grown by MBE, the MOCVD grown

Optics EXPRESS

1.5 μm lasers are much less mature and have room for improvement, in both the InP/Si templates and QDash growth technologies. The life time of the MOCVD grown 1.5 μm lasers is also a topic for future investigation [2].

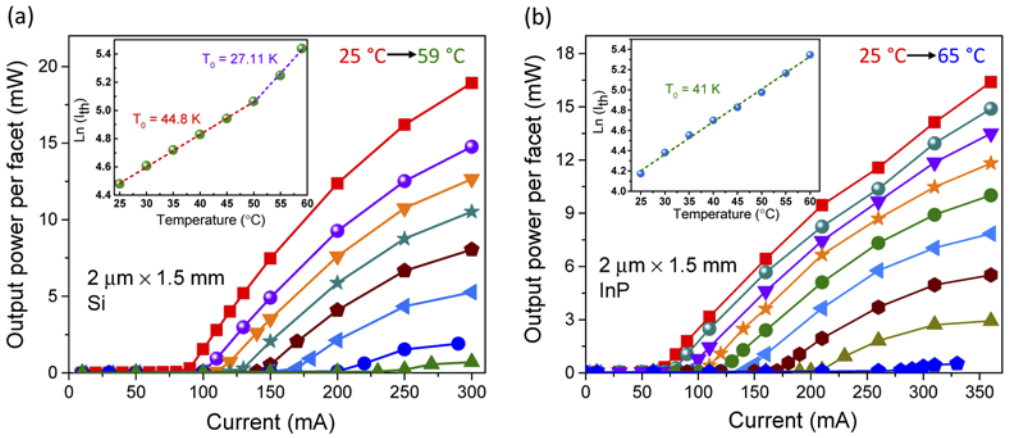

Fig. 5. (a) Temperature-dependent measurement results of lasers on Si with characteristic temperature presented in the inset; (b) High temperature L-I curves of lasers on InP with the fitting curve for extracting characteristic temperature shown in the inset.

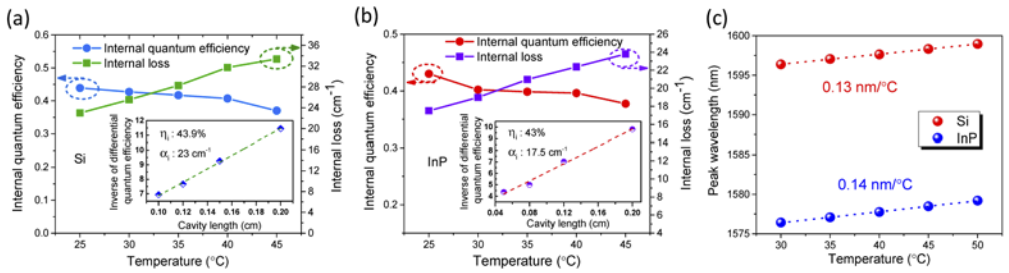

Fig. 6. Temperature-dependent parameters, (a) Extracted IQE and internal loss against varied temperatures of lasers on Si with 4 μm cavity width, inset: inverse differential quantum efficiency versus cavity length with derived IQE and internal loss at 25 °C; (b) Calculated IQE and internal absorption of lasers on InP with 2 μm cavity width plotted as function of temperature, inset: linear fitting curve of the relation of inverse differential quantum efficiency and different cavity lengths with extracted IQE and internal loss at 25 °C; (c) Shift of the primary lasing peak with increase of temperature for the QDash lasers (2 μm × 1.5 mm) grown on the two substrates.

4. Conclusion

In conclusion, we report the first room temperature CW lasing results of QDash lasers grown on Si by MOCVD emitting at 1.55 μm. By adopting a dash-in-well structure and improved high quality QDashes in material growth as well as deep etched structure in device fabrication, the lowest threshold of 50 mA, lowest threshold current density of 1.3 kA/cm^2 and CW lasing sustain up to 59 °C were demonstrated. The comparison of QDash lasers on Si and native InP substrates led to the conclusion that the overall performance of the lasers on these two substrates are comparable. The results reported in this work demonstrate significant improvement from our

Optics EXPRESS

previously reported results [23,25]. These record results promise the III-V-On-Si light source and propel the realization of fully integrated photonic circuits on the silicon platform.

Funding

Research Grants Council, University Grants Committee (614813, 16212115); Innovation and Technology Fund (ITS/273/16FP).

Acknowledgments

The authors would like to thank the MCPF and NFF of HKUST for technical support. Helpful discussions with Peter M. Smowton and Yating Wan are also acknowledged.

Disclosures

The authors declare no conflicts of interest.

References

1. Q. Feng, W. Wei, B. Zhang, H. Wang, J. Wang, H. Cong, T. Wang, and J. Zhang, "O-Band and C/L-Band III-V Quantum Dot Lasers Monolithically Grown on Ge and Si Substrate," Appl. Sci. **9**(3), 385 (2019).
2. S. Chen, W. Li, J. Wu, Q. Jiang, M. Tang, S. Shutts, S. N. Elliot, A. Sobiesierski, A. J. Seeds, I. Ross, P. M. Smowton, and H. Liu, "Electrically pumped continuous-wave III–V quantum dot lasers on silicon," Nat. Photonics **10**(5), 307–311 (2016).
3. J. C. Norman, D. Jung, Y. Wan, and J. E. Bowers, "Perspective: The future of quantum dot photonic integrated circuits," APL Photonics **3**(3), 030901 (2018).
4. D. Thomson, A. Zilkie, J. E. Bowers, T. Komljenovic, G. T. Reed, L. Vivien, D. Marris-Morini, E. Cassan, L. Virot, J.-M. Fédéli, J.-M. Hartmann, J. H. Schmid, D.-X. Xu, F. Boeuf, and P. O'Brien, "Goran Z Mashanovich1 and M Nedeljkovic, "Roadmap on silicon photonics"," J. Opt. **18**(7), 073003 (2016).
5. K. Lia, Z. Liua, M. Tanga, M. Liaoa, D. Kima, H. Denga, A. M. Sanchezb, R. Beanlandb, M. Martinc, T. Baronc, S. Chena, J. Wua, A. Seedsa, and H. Liu, "O-band InAs/GaAs quantum dot laser monolithically integrated on exact (001) Si substrate," J. Cryst. Growth **511**, 56–60 (2019).
6. E. Moiseev, N. Kryzhanovskaya, M. Maximov, F. Zubov, A. Nadtochiy, M. Kulagina, Y. Zadiranov, N. Kalyuzhnyy, S. Mintairov, and A. Zhukov, "Highly efficient injection microdisk lasers based on quantum well-dots," Opt. Lett. **43**(19), 4554–4557 (2018).
7. D. L. Chong Zhang, G. Kurczveil, A. Descos, and R. G. Beausoleil, "Hybrid quantum-dot microring laser on silicon," Optica **6**(9), 1145–1151 (2019).
8. J. Norman, M. J. Kennedy, J. Selvidge, Q. Li, Y. Wan, A. Y. Liu, P. G. Callahan, M. P. Echlin, T. M. Pollock, K. M. Lau, A. C. Gossard, and J. E. Bowers, "Electrically pumped continuous wave quantum dot lasers epitaxially grown on patterned, on-axis (001) Si," Opt. Express **25**(4), 3927–3934 (2017).
9. Y. Han, Y. Xue, and K. M. Lau, "Selective lateral epitaxy of dislocation-free InP on silicon-on-insulator," Appl. Phys. Lett. **114**(19), 192105 (2019).
10. S. Shutts, C. P. Allford, C. Spinnier, Z. Li, A. Sobiesierski, M. Tang, H. Liu, and P. Smowton, "Degradation of III–V Quantum Dot Lasers Grown Directly on Silicon Substrates," IEEE J. Sel. Top. Quantum Electron. **25**(6), 1–6 (2019).
11. C. Shang, Y. Wan, J. C. Norman, N. Collins, I. MacFarlane, M. Dumont, S. Liu, Q. Li, K. M. Lau, A. C. Gossard, and J. E. Bowers, "Low-Threshold Epitaxially Grown 1.3-μm InAs Quantum Dot Lasers on Patterned (001) Si," IEEE J. Sel. Top. Quantum Electron. **25**(6), 1–7 (2019).
12. J. C. Norman, D. Jung, Z. Zhang, Y. Wan, S. Liu, C. Shang, R. W. Herrick, W. W. Chow, A. C. Gossard, and J. E. Bowers, "A Review of High-Performance Quantum Dot Lasers on Silicon," IEEE J. Quantum Electron. **55**(2), 1–11 (2019).
13. Bei Shi, Hongwei Zhao, Lei Wang, Bowen Song, Simone Tommaso, Suran Brunelli, and Jonathan Klamkin, "Continuous-wave electrically pumped 1550 nm lasers epitaxially grown on on-axis (001) silicon," Optica **6**(12), 1507–1514 (2019).
14. A. Y. Liu, S. Srinivasan, J. Norman, A. C. Gossard, and J. E. Bowers, "Quantum dot lasers for silicon photonics," Photonics Res. **3**(5), B1–B9 (2015).
15. M. Liao, S. Chen, Z. Liu, Y. Wang, L. Ponnampalam, Z. Zhou, J. Wu, M. Tang, S. Shutts, Z. Liu, P. M. Smowton, S. Yu, A. Seeds, and H. Liu, "Low-noise 1.3 μm InAs/GaAs quantum dot laser monolithically grown on silicon," Photonics Res. **6**(11), 1062–1066 (2018).
16. Y. Wan, D. Inoue, D. Jung, J. C. Norman, C. Shang, A. C. Gossard, and J. E. Bowers, "Directly modulated quantum dot lasers on silicon with a milliampere threshold and high temperature stability," Photonics Res. **6**(8), 776–781 (2018).

Optics EXPRESS

17. J. Kwoen, B. Jang, K. Watanabe, and Y. Arakawa, "High-temperature continuous-wave operation of directly grown InAs/GaAs quantum dot lasers on on-axis Si (001)," Opt. Express **27**(3), 2681–2688 (2019).
18. B. Shi, Y. Han, Q. Li, and K. M. Lau, "1.55-μm Lasers Epitaxially Grown on Silicon," IEEE J. Sel. Top. Quantum Electron. **25**(6), 1–11 (2019).
19. Y. Han, W. K. Ng, Y. Xue, Q. Li, K. S. Wong, and K. M. Lau, "Telecom InP/InGaAs nanolaser array directly grown on (001) silicon-on-insulator," Opt. Lett. **44**(4), 767–770 (2019).
20. S. Zhu, B. Shi, and K. M. Lau, "Electrically pumped 1.5 μm InP-based quantum dot microring lasers directly grown on (001) Si," Opt. Lett. **44**(18), 4566–4569 (2019).
21. Y. Han, W. K. Ng, Y. Xue, K. S. Wong, and K. M. Lau, "Room temperature III–V nanolasers with distributed Bragg reflectors epitaxially grown on (001) silicon-on-insulators," Photonics Res. **7**(9), 1081–1086 (2019).
22. Q. Li, Y. Wan, A. Y. Liu, A. C. Gossard, J. E. Bowers, E. L. Hu, and K. M. Lau, "1.3-μm InAs quantum-dot micro-disk lasers on V-groove patterned and unpatterned (001) silicon," Opt. Express **24**(18), 21038–21045 (2016).
23. S. Zhu, B. Shi, Q. Li, and K. M. Lau, "1.5 μm quantum-dot diode lasers directly grown on CMOS-standard (001) silicon," Appl. Phys. Lett. **113**(22), 221103 (2018).
24. A. A. Ukhanov, R. H. Wang, T. J. Rotter, A. Stintz, L. F. Lester, P. G. Eliseev, and K. J. Malloy, "Orientation dependence of the optical properties in InAs quantum-dash lasers on InP,"," Appl. Phys. Lett. **81**(6), 981–983 (2002).
25. S. Zhu, B. Shi, Q. Li, and K. M. Lau, "Room-temperature electrically-pumped 1.5 μm InGaAs/InAlGaAs laser monolithically grown on on-axis (001) Si," Opt. Express **26**(11), 14514–14523 (2018).
26. A. Abdollahinia, S. Banyoudeh, A. Rippien, F. Schnabel, O. Eyal, I. Cestier, I. Kalifa, E. Mentovich, G. Eisenstein, and J. P. Reithmaier, "Temperature stability of static and dynamic properties of 1.55 μm quantum dot lasers," Opt. Express **26**(5), 6056–6066 (2018).
27. C. Gilfert, V. Ivanov, N. Oehl, M. Yacob, and J. P. Reithmaier, "High gain 1.55 μm diode lasers based on InAs quantum dot like active regions," Appl. Phys. Lett. **98**(20), 201102 (2011).
28. F. I. Zubov, S. P. Gladii, Y. M. Shernyakov, M. V. Maximov, E. S. Semenova, I. V. Kulkova, K. Yvind, and A. E. Zhukov, "1.5 μm InAs/InGaAsP/InP quantum dot laser with improved temperature stability," J. Phys.: Conf. Ser. **741**, 012109 (2016).
29. V. I. Sichkovskyi, M. Waniczek, and J. P. Reithmaier, "High-gain wavelength-stabilized 1.55 μm InAs/InP (100) based lasers with reduced number of quantum dot active layers," Appl. Phys. Lett. **102**(22), 221117 (2013).
30. Y. Wan, D. Jung, C. Shang, N. Collins, I. MacFarlane, J. Norman, M. Dumont, A. C. Gossard, and J. E. Bowers, "Low-Threshold Continuous-Wave Operation of Electrically Pumped 1.55 μm InAs Quantum Dash Microring Lasers," ACS Photonics **6**(2), 279–285 (2019).
31. S. G. Li, Q. Gong, C. F. Cao, X. Z. Wang, J. Y. Yan, and Y. Wang, "Thermal coefficient of InP-based quantum dot laser from cavity-mode measurements," Infrared Phys. Technol. **68**, 119–123 (2015).